Free Volume Analysis and Gas Transport Mechanisms of Aromatic Polyimide Membranes: A Molecular Simulation Study

Kai-Shiun Chang, Chieng-Chi Tung, Ko-Shung Wang, and Kuo-Lun Tung*

R&D Center of Membrane Technology, and Department of Chemical Engineering, Chung Yuan Christian University, Chung-Li, Taoyuan 320, Taiwan

Received: April 17, 2009; Revised Manuscript Received: May 23, 2009

Molecular simulation techniques were adopted to investigate membrane free volume morphologies and gas-transport mechanisms in the aromatic polyimide (PI) membranes composed of various diamines and dianhydrides. A molecular dynamics (MD) technique was adopted to analyze the fractional free volume (FFV), fractional accessible volume (FAV), free volume size and shape, and diffusion mechanisms. A Monte Carlo (MC) method was used to analyze the gas sorption behaviors in the membranes. The FFV, FAV, and free volume morphology analyses reveal that bulky groups in the PI membranes contributed to the formation of a larger and more continuous free volume. The thermal motion analysis shows that a greater effective free volume in the membranes promoted effective motion, such as jumping and diffusive motions. The sorption analysis indicates that the larger free volume provides more sites for gas molecule absorption. The MD and MC results provide good agreement with the experimental data from past reports, which validates the feasibility of molecular simulation techniques in gas separation membranes at a molecular scale.

1. Introduction

Membrane technology is regarded as a simple and efficient technique for gas separation. The nature of the selected materials and fabrication parameters dominate the characteristics of the prepared polymeric membranes. On the other hand, past studies have focused on the effect of casting solvent types and residual solvents on the membrane free volume and its performance.[1−12] Moreover, some researchers have investigated the effect of the polymer species configuration, including the side chain composition and main chain structure, on the membrane performance.[9,13−28] For instance, the tacticity of poly(methyl methacrylate) (PMMA) would obviously affect the membrane free volume and its gas permeability.[13] Past reports have also pointed out that the addition of bulky CF_3 groups in polyimide (PI) results in a good gas permeability and selectivity.[8] Further, Hofmann et al.[14] fabricated perfluorinated polymeric membranes containing different percentages of tetrafluoroethylene (TFE). In their report, they adopted positron annihilation lifetime spectroscopy (PALS) to analyze the membrane free volume and compared these data with the gas permeability. It was found that the membranes containing more TFE structures provided much greater voids and gas permeability. Hirayama et al.[15,16] synthesized 32 kinds of PI membranes composed of different diamines and dianhydrides to evaluate their gas permeability. They analyzed the cohesive energy density (CED) of PI membranes and correlated these CED values with the diffusion coefficients. From their analyses, they suggested that polymer chains containing polar substituents would change the segment mobility and then control the gas diffusion mechanisms. Wang et al.[17] also fabricated seven kinds of aromatic PI membranes composed of various diamines and dianhydrides. They noted that the bulky groups inhibited polymer chain packing and then formed a larger fractional free volume (FFV) in the membranes. The increased FFV of the membrane prompted higher gas permeability. Liu et al.[18] prepared mono-PI, 6FDA−durene, 6FDA−2,6-diaminotoluene (2,6-DAT), and co-PI, 6FDA-durene/2,6-DAT membranes with various diamine ratios. They found that the increase in 6FDA−2,6-DAT in co-PI decreased the gas diffusivity and solubility, resulting in improved intrasegment packing, which lowered the gas permeation.

Today, molecular simulation techniques supply a new potential method for obtaining an in-depth understanding on a molecular scale.[9−11,14,23,29−33] Smit et al.[29] analyzed the motion types of gas molecules in PI membranes using a molecular dynamics (MD) simulation. Two different types of diffusion behavior, residual time and flying time, in the membrane were observed. In addition, an increase in the temperature raised the small-molecule thermal motion and thus contributed to a higher diffusivity.[30] Tung et al.[9−11] investigated the effect of PMMA tacticity and casting solvent types on free volume morphology and the gas transport mechanisms using MD and Monte Carlo (MC) techniques. Their simulated values coincided well with the experimental data. Heuchel et al.[32] simulated the gas permeability, solubility, and diffusivity of O_2 and N_2 in PI membranes. Moreover, past studies[14,21,23] have analyzed the free volume distribution using MD simulations and PALS analysis. They investigated the effect of various backbone stiffness values and substituent types on the membrane structure, gas solubility, and diffusion coefficient.

From the above reports, it has been indicated that the polymer composition and functional groups clearly dominate membrane structure and performance. However, the effect of the functional group (or substituent group) on the free volume size and shape distribution and transport mechanisms still remains elusive at a molecular scale. In this study, the free volume morphology and gas diffusion mechanisms of seven kinds of aromatic PI membranes composed of various diamines and dianhydrides were analyzed via an MD technique. The gas sorption behaviors in different membranes under various operation pressures were also investigated using the MC technique. To validate the feasibility and accuracy of this simulated work, all of the calculated results were compared with the experimental data of Wang et al.[17] (FFV and O_2- and N_2-transport behaviors).

* To whom correspondence should be addressed. Tel: +886-3-2654129. Fax: +886-3-2654199. E-mail: kuolun@cycu.edu.tw.

10.1021/jp903551h CCC: $40.75
Published on Web 07/01/2009

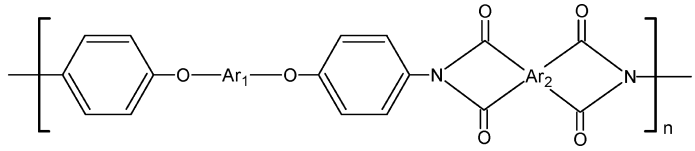

(a)

Ar_1	Ar_2			
BATB	6FDA	BPDA	BTDA	DSDA
TMBPS	6FDA	ODPA	BTDA	

(b)

Figure 1. Scheme of (a) an aromatic polyimide monomer and (b) the adopted aromatic groups.

TABLE 1: Physical Properties of Aromatic PI Membranes from Wang et al.[17]

PI membrane	ρ (g/cm^3)	T_g (°C)
BATB−6FDA	1.35	248
BATB−BPDA	1.27	261
BATB−BTDA	1.29	247
BATB−DSDA	1.33	246
TMBPS−6FDA	1.34	304
TMBPS−ODPA	1.30	291
TMBPS−BTDA	1.30	295

2. Theoretical Methods

This work investigated the effect of different diamines and dianhydrides in PI membranes on the free volume morphology and gas transport behaviors. All of the molecular models in this study were built by the Cerius^2 package from Accelrys (originally MSI). All of the queuing calculations were carried out at the National Center for High-Performance Computing (NCHC), Taiwan. All of the physical properties for the molecular model construction were adopted from Wang et al.[17] The procedures of model building and property analyses are described in the following paragraphs.

2.1. Model Construction. In our work, the models of aromatic PI membranes were composed of different diamines and dianhydrides. Two categories of membrane models were fabricated, 1,4-bis(4-aminophenoxy)-2-*tert*-butylbenzene-based PI membranes (BATA-based PI membranes) and 3,3′,5,5′-tetramethyl-bis[4-(4-aminophenoxy)phenyl]sulfone-based PI membranes (TMBPS-based PI membranes). Figure 1 shows the monomer of a selected PI and the units of various diamines and dianhydrides. The number of repeating units of our molecular models was set at 15 to optimize the trade-off between cell dimension and calculation time. In model building, the periodical boundary condition was also adopted for eliminating the wall effect. Table 1 lists the membrane density and glass transformation temperature (T_g) of the aromatic PI membranes from Wang et al.[17] All of the molecular models were processed with an energy minimization step over 1000 iterations to obtain a stable structure. Then, the MD calculations were performed under an *NVT* ensemble (fixed number of atoms, cell volume, and temperature) for the duration of 1 ns at 308 K. The Newton second law of motion was employed to calculate the dynamic behaviors of molecules in our model. The modified Verlet algorithm was adopted for integration in our MD simulation.

2.2. Compass Force Field. In our work, the Compass force field (condensed-phase optimized molecular potential for atomistic simulation studies) was adopted for the theoretical calculations. There are three types of energy terms, the bonded energy terms, the cross terms, and the nonbonded energy terms. The bonded energy terms consist of (a) the covalent bond stretching energy terms, (b) the bond angle bending energy terms, and (c) the torsion angle rotation energy terms of the polymer chain. The energy of the torsion angle was fitted by a Fourier series function. The out-of-plane energy, or improper term (d), is described as a harmonic function. The terms of the cross interaction include the dynamic variation among the bond stretching, bending, and torsion angle rotation (e−j). The last two terms, (k) and (l), represent the Coulomb electrostatic force and van der Waals force, respectively, which are interactive forces between polymer chains and solvent molecules.

$$
\begin{aligned}
E = {} & \sum_b \left[K_2 (b-b_0)^2 + K_3 (b-b_0)^3 + K_4 (b-b_0)^4 \right] \\
& \text{(a)} \\
& + \sum_\theta \left[H_2 (\theta-\theta_0)^2 + H_3 (\theta-\theta_0)^3 + H_4 (\theta-\theta_0)^4 \right] \\
& \text{(b)} \\
& + \sum_\phi \left\{ V_1 \left[1-\cos\left(\phi-\phi_1^0\right) \right] + V_2 \left[1-\cos\left(2\phi-\phi_2^0\right) \right] + V_3 \left[1-\cos\left(3\phi-\phi_3^0\right) \right] \right\} \\
& \text{(c)} \\
& + \sum_x K_x x^2 + \sum_b \sum_{b'} F_{bb'} (b-b_0)(b'-b'_0) + \sum_\theta \sum_{\theta'} F_{\theta\theta'} (\theta-\theta_0)(\theta'-\theta'_0) \\
& \text{(d)} \qquad \text{(e)} \qquad \text{(f)} \\
& + \sum_b \sum_\theta F_{b\theta} (b-b_0)(\theta-\theta_0) + \sum_b \sum_\phi (b-b_0)\left[V_1 \cos\phi + V_2 \cos 2\phi + V_3 \cos 3\phi \right] \\
& \text{(g)} \qquad \text{(h)} \\
& + \sum_{b'} \sum_\phi (b'-b'_0)\left[V_1 \cos\phi + V_2 \cos 2\phi + V_3 \cos 3\phi \right] \\
& \text{(i)} \\
& + \sum_\phi \sum_\theta \sum_{\theta'} K_{\phi\theta\theta'} \cos\phi (\theta-\theta_0)(\theta'-\theta'_0) + \sum_{i>j} \frac{q_i q_j}{\varepsilon r_{ij}} + \sum_{i>j} \left[2\left(\frac{A_{ij}}{r_{ij}^9}\right) - 3\left(\frac{B_{ij}}{r_{ij}^6}\right) \right] \qquad (1) \\
& \text{(j)} \qquad \text{(k)} \qquad \text{(l)}
\end{aligned}
$$

2.3. Physical Properties. ***Fractional Free Volume.*** The fractional free volume (FFV) and van der Waals volume (V_W) of a membrane can be calculated by the following equations

$$\mathrm{FFV} = \frac{V - V_0}{V} \tag{2}$$

$$V_0 = 1.3V_W \tag{3}$$

where V_W is obtained from the van der Waals surface instead of using Bondi's groups. The accessible volume and fractional accessible volume (FAV) were obtained using a hard spherical particle to probe the available volume for a particle passing through. The cross sections of the cubic membrane model in the x, y, and z directions were analyzed for the free volume morphology analysis. The image of the cross section was treated as a photo composed of 256 pixels × 256 pixels. The areas occupied by the free volume in the cross-sectional image were calculated and transformed to equivalent diameters. Then, the free volume size distribution was obtained by counting the free volume equivalent diameters.

Sorption and Diffusion Mechanisms. The process of gas molecule sorption in a membrane can be divided into three steps, as follows: (1) the molecule is absorbed in the membrane matrix, (2) the absorbate reacts or exchanges sorption sites in the membrane matrix, and (3) the absorbate desorbs from the membrane matrix. In the present work, MC simulations were used to correctly calculate and illustrate the three sorption mechanisms. Here, the sorption interface behaviors were simulated using the grand canonical Monte Carlo method (GCMC). In addition, the gas concentration probability in the membrane matrix was determined by the energy change between the new configuration and the previous one. In this procedure, the acceptance or rejection of the configurational movements of sorbate molecules was decided using the Metropolis algorithm. There are four types of configurational movements, including creation, rotation, translation, and destruction. The creation and destruction probabilities of the movements of sorbate molecules can be expressed as

$$P = \min\left[1;\exp\left(-\frac{\Delta E}{kT} \pm \ln\frac{(N_i + 1)kT}{f_i V}\right)\right] \tag{4}$$

where ΔE is the energy change between the new configuration and the previous one, k is Boltzmann's constant, T is the assigned simulation temperature, N_i is the number of the component i molecule in the configuration, f is the fugacity of the component i molecule, and V is the cell volume. The probability of translational movement in the membrane cell is

$$P = \min\left[1;\exp\left(-\frac{\Delta E}{kT}\right)\right] \tag{5}$$

All four kinds of the aforementioned probabilities were calculated and considered as a complete MC calculation step. The sorption analysis calculation in this work was processed 1 000 000 times. The number of accepted sorption configurations was recorded and calculated as the sorption loading.

The gas diffusion mechanisms in the membrane were classified into three categories, thermal diffusive, jumping, and trapped motion. The classification was mainly dominated by

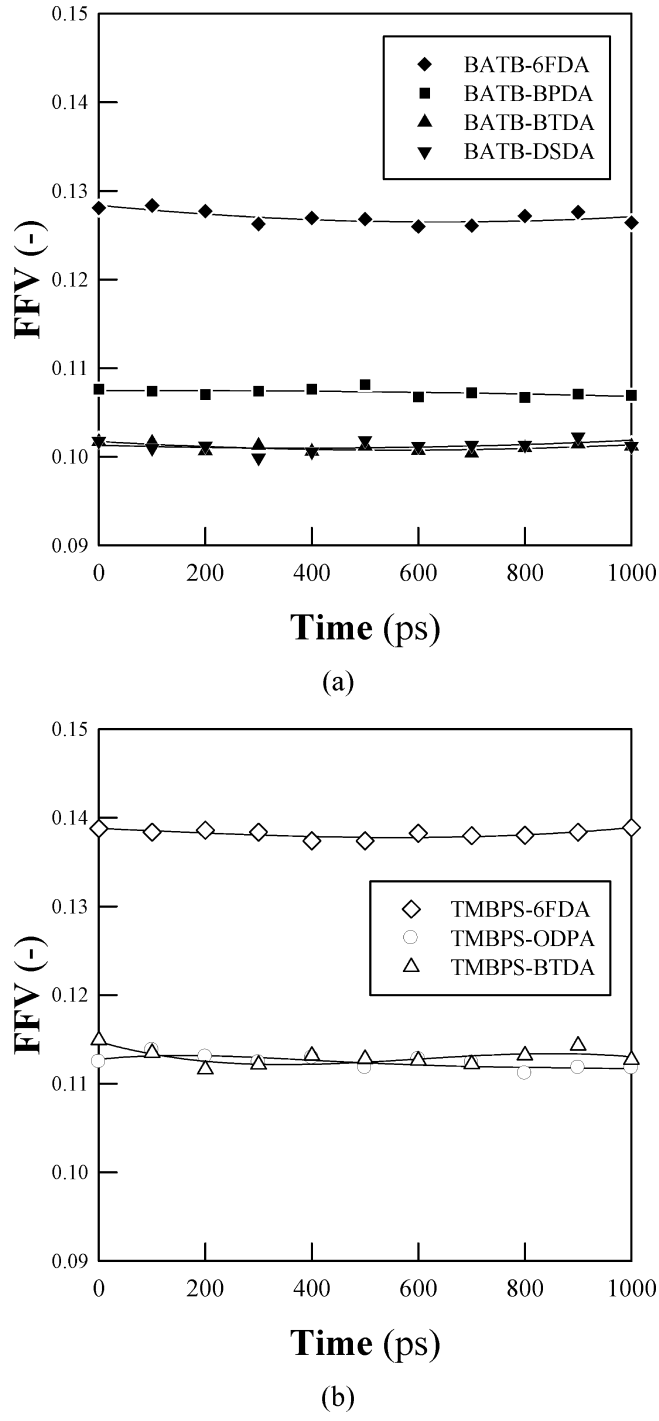

Figure 2. The fractional free volume of BATB-based and TMBPS-based PI membranes over 1000 ps.

the average radius or diameter of the atoms, as calculated from their van der Waals volumes in the membrane. The diffusion mechanism of the gas molecules was classified as thermal jumping if the value of the molecule's mean-squared distance (MSD) was larger than the average radius (R_{eq}^2) or the average diameter (D_{eq}^2) during the specific time duration, where the average radius and diameter could be expressed as

$$R_{eq} = \left(\frac{3}{4}\frac{\sum_{i=1}^{n} V_{W,i}}{n\pi}\right)^{1/3} \quad \text{and} \quad D_{eq} = 2\left(\frac{3}{4}\frac{\sum_{i=1}^{n} V_{W,i}}{n\pi}\right)^{1/3} \tag{6}$$

TABLE 2: The Experimental and Simulated FFV Values of Aromatic PI Membranes

PI membrane	$FFV_{Sim.}$ (−)	$FFV_{Exp.}$[a] (−)
BATB−6FDA	0.156	0.127
BATB−BPDA	0.133	0.107
BATB−BTDA	0.129	0.101
BATB−DSDA	0.123	0.101
TMBPS−6FDA	0.159	0.138
TMBPS−ODPA	0.136	0.113
TMBPS−BTDA	0.132	0.112

[a] From Wang et al.[17]

To analyze the diffusive mechanism, the slope of the five continuous MSD values was calculated using the least-squares method. The mechanism was considered to be of a diffusive type if the value of the slope was less than 0.5. Finally, the probability of the trapped mechanism was obtained by subtracting the probabilities of the thermal jumping and diffusion from unity.

3. Results and Discussion

3.1. Fractional Free Volume (FFV) and Fractional Accessible Volume (FAV). ***Fractional Free Volume.*** Figure 2 illustrates the FFV of BATB-based and TMBPS-based PI membranes for the duration of 1000 ps. The lack of apparent FFV variance in all of the PI membrane FFV values during the 1000 ps duration indicates that the membrane structure has approached a stable equilibrium state. In the case of BATB-based PI membranes, it was found that the BATB−6FDA PI membrane had an obviously higher FFV value than all of the other membranes. This tendency for a larger FFV suggests that the bulky 6FDA group in the polymer inhibited the polymer chain packing and formed a free space in the membrane matrix. In addition, we found that the FFV values of the BATB−BPDA and BATB−DSDA PI membranes nearly overlapped. This result of similar FFV values could be attributed to the similar geometric shape of the aromatic group structure. In the case of TMBPS-based PI membranes, we found the same tendency for a higher FFV value, resulting from the bulky 6FDA group, in the TMBPS−6FDA PI membrane. Furthermore, it was found that the TMBPS-based PI membranes exhibited larger FFV values than the BATB-based PI membranes. This clear increase in FFV value indicates that the larger TMBPS group has a much greater influence on the polymer configuration than the BATB group and controls the membrane free volume. On the other hand, we also observed that there was no clear variance between the TMBPS−ODPA and TMBPS−BTDA PI membranes, although they contained different dianhydride groups. The reason for this similar FFV value was attributed to the much greater influence of the bulky TMBPS group in the membrane matrix, which eliminated the structure effect of the ODPA and BTDA groups on the overall free volume. Table 2 lists the experimental and simulated FFV values of the aromatic PI membranes. It was found that the results of the experimental and simulated data are quite close. These similar FFV values validate the feasibility of the MD technique for polymeric membrane analysis with accurate results. Thus, the free volume may be controlled by the selected aromatic group of the PI membranes. However, the FFV value might not provide accurate information about gas molecules passing through the membrane. In other words, the FFV value only indicated the overall free region but not the effective space for specific species penetration. Hence, the fractional accessible volume (FAV) and free volume morphology will be discussed for deeper understanding in the following paragraphs.

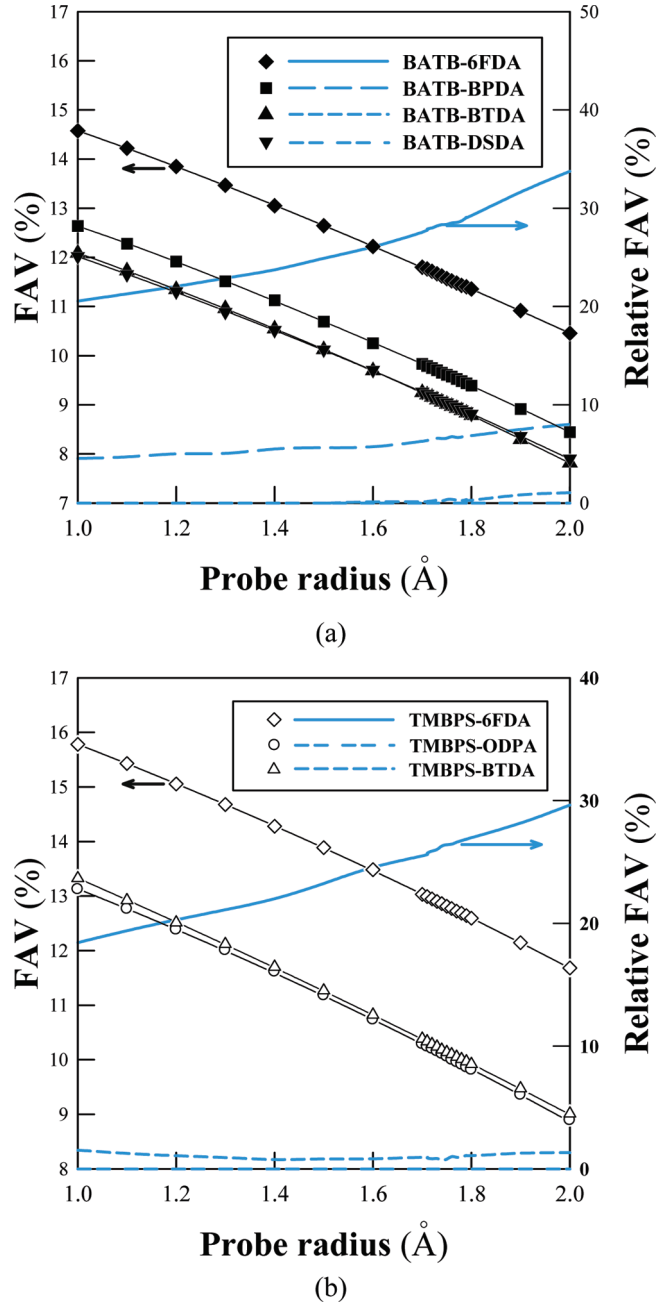

Figure 3. The FAV and relative FAV values of (a) BATB-based PI membranes and (b) TMBPS-based PI membranes, probed by probes with different radii.

Fractional Accessible Volume. Figure 3 illustrates the FAV values of BATB-based and TMBPS-based PI membranes probed by probes with different radii, ranging from 1.1 to 2.0 Å. The probe radii close to the radii of N_2 (1.73 Å) and CO_2 (1.86 Å) are found within this range for comparison with the gas permeability data from experimental results.[17] In the FAV analysis, we found similar results with the FFV analysis that we mentioned above, as illustrated by the following: (1) the 6FDA group decreased the polymer chain packing efficiency, thus forming a larger free volume, and (2) the TMBPS group had a larger influence on the free volume than the BATB group in the PI membrane. In addition, we also observed similar tendencies in both the experimental and simulated results. Thus, the PI membranes with a higher free volume were found to provide effective free space for gas transport. We also calculated the relative FAV of the PI membranes, compared with the lowest

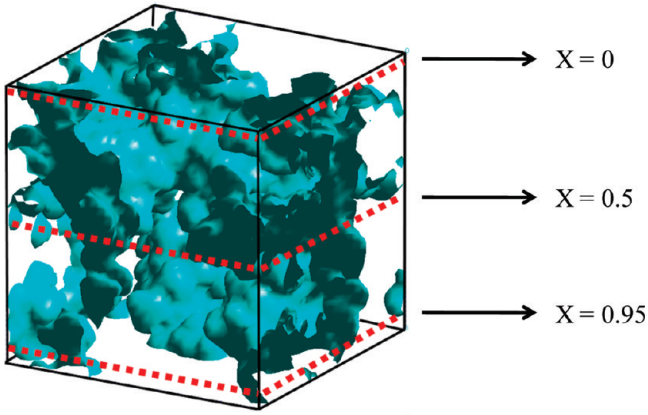

Figure 4. Selected cross sections of the molecular model in the *x*-direction.

FAV values of the BATB-based and TMBPS-based PI membranes, respectively, as follows

$$\frac{\text{FAV(BATA-based PI)} - \text{FAV(BATB}-\text{DSDA)}}{\text{FAV(BATB}-\text{DSDA)}} \times 100\% \quad (7)$$

or

$$\frac{\text{FAV(TMBPS-based PI)} - \text{FAV(TMBPS}-\text{ODPA)}}{\text{FAV(TMBPS}-\text{ODPA)}} \times 100\% \quad (8)$$

Figure 3 shows the relative FAV values of the PI membranes. It was found that the PI membranes containing the 6FDA group had much higher relative FAV values than all of the other membranes, which increased as the probe radius increased. This remarkable difference in the FAV value shows that the 6FDA group has a strong effect on the useful free volume quantity, as compared to all of the other aromatic groups used in this work. Meanwhile, the effect on the effective free volume tended to increase as the probe size increased, which was considered to contribute to gas diffusion or sorption.

3.2. Free Volume Morphology Analysis. To understand how the free volume element is distributed in the membrane matrix, we analyzed the free volume morphology, including size and shape, using an image analysis method. In this image analysis, we selected three positions of membrane cross sections in the *x*-direction to analyze the free volume morphology, as shown in Figure 4. The equivalent diameters (D_{eq}) of the free area in the cross-sectional image were calculated using Matlab. Later, the free volume size distribution (FVSD) was obtained by collecting the statistics of the counts and values of D_{eq} from the cross-sectional images. In the case of free volume shape analysis, the free volume area in the image was transformed to an equivalent ellipse with an equivalent eccentricity value ($E_{eq} = a/c$, where a is the length of the semimajor axis and c is the distance from the foci to the center). As the eccentricity approaches 0, the shape of the free area in the image approaches a circle. On the other hand, if the eccentricity approaches unity, the shape of the free area approaches a line.

In the free volume size analysis, both quantitative and qualitative analyses were adopted. Figure 5 show the results of the quantitative FVSD analysis of the BATB-based and TMBPS-based PI membranes. In the FVSD analysis, we found that more than 90% of the free volume elements had D_{eq} values located

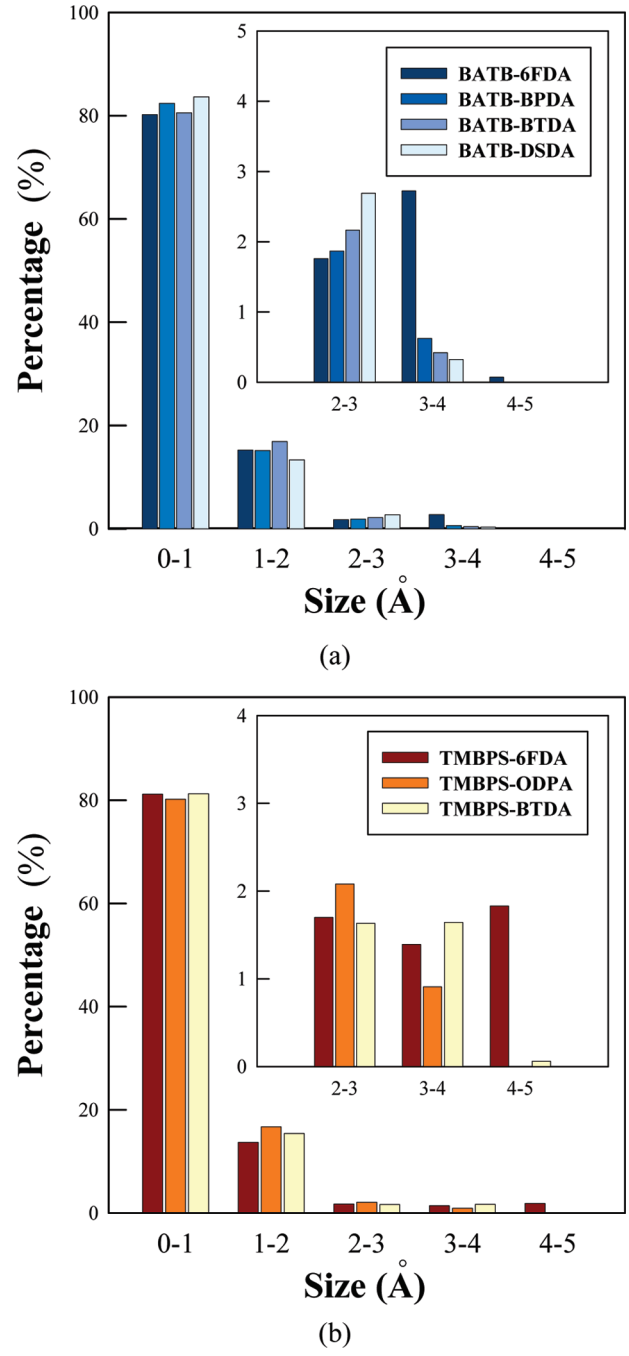

Figure 5. The size distribution of free volume equivalent diameters of (a) BATB-based PI membranes and (b) TMBPS-based PI membranes.

in the range of 0−3 Å. Concerning N_2 and O_2 transport, those small free volume elements were considered to be useless for transporting gas molecules. This result suggests that the PI membrane could be categorized as a dense membrane for gas separation. Thus, the appearance of apparently larger or more continuous free space in this type of membrane might have a great effect on gas diffusion or sorption behavior. For O_2 and N_2 transport, free volume elements with a D_{eq} value larger than 3 Å might be effective in enhancing the gas permeability. Regarding the D_{eq} values greater than 3 Å in Figure 5, the 6FDA-containing PI membranes had a higher percentage of D_{eq} values than all of the other BATB-based and TMBPS-based PI membranes, in the following order: BATB−6FDA > BATB−BPDA > BATB−BTDA > BATB−DSDA and TMBPS−6FDA > TMBPS−BTDA > TMBPS−ODPA. The 6FDA-containing PI

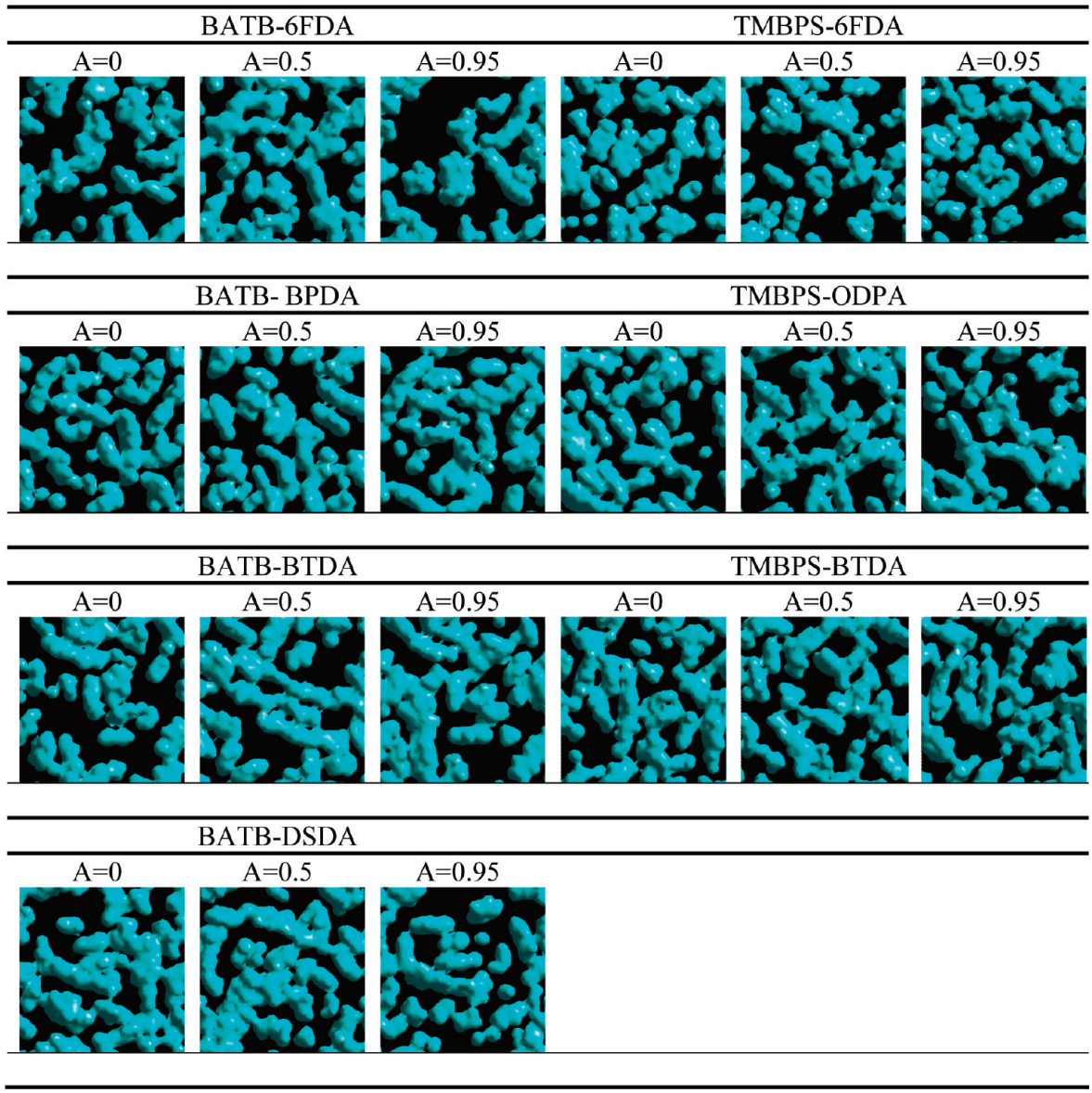

Figure 6. Free volume cross section of BATB-based and TMBPS-based PI membranes at thickness = 1.5 Å. ($A = x/a$, where a is the cell length in the amorphous model and x is the free volume cross section position in the x-direction.)

membrane had a larger or more continuous free volume than all of the other membranes. This tendency for a higher free volume D_{eq} value in 6FDA-containing PI membranes is in agreement with the FFV and FAV analyses above.

In the case of BATB-based PI membrane, the bulky 6FDA group inhibited the polymer chain packing, resulting in the largest free volume. Regarding the BPDA group, it was composed of two continuous connected benzenes, which revealed a higher stiffness than BTDA and DSDA groups, forming the largest free volume next to the 6FDA group. Considering the BTDA and DSDA groups, they had clearly lower molecular volumes compared to the 6FDA group, which leads to the higher packing efficiency and obviously less free volume. However, the BATB−DSDA PI membrane had a larger dianhydride group than the BATB−BTDA PI membrane but revealed a lower effective free volume. This opposite tendency of substituent group volume and free volume values can be explained by the following illustrations. Since the BTDA and DSDA groups provided the higher packing efficiency of polymer chains, the side oxygen atoms of the DSDA group might have also suppressed the side chain fluctuation because of the steric hindrance, which probably caused the lower free space in the membrane. The results of Wang et al.[17] revealed that the 6FDA−BTDA polyimide membrane possesses a lower γ-transition temperature than 6FDA−DSDA polyimide membrane, which indicated that the mobility of local polymer segments in 6FDA−BTDA polyimide was higher than the 6FDA−DSDA polyimide membrane, causing the higher free volume. Meanwhile, we can also find similar results in FVSD analysis from our simulation and experimental work as Wang et al.,[17] which validates the correctness of the simulation work. Moreover, the similar tendency was also observed in the case of TMBPS-based polyimide membranes.

However, the trend of TMBPS−ODPA and TMBPS−BTDA in the FFV analysis (without a definite order of magnitude) differed from that of the FAV analysis (TMBPS−BTDA > TMBPS−ODPA), while the FAV results revealed a better agreement with the experimental data. This indicates that the FAV analysis provided a more accurate method for effective free volume investigation. Meanwhile, the FVSD analysis also suggested the same trend as the FAV data. The TMBPS−BTDA had a higher percentage of free volume D_{eq} values in the range

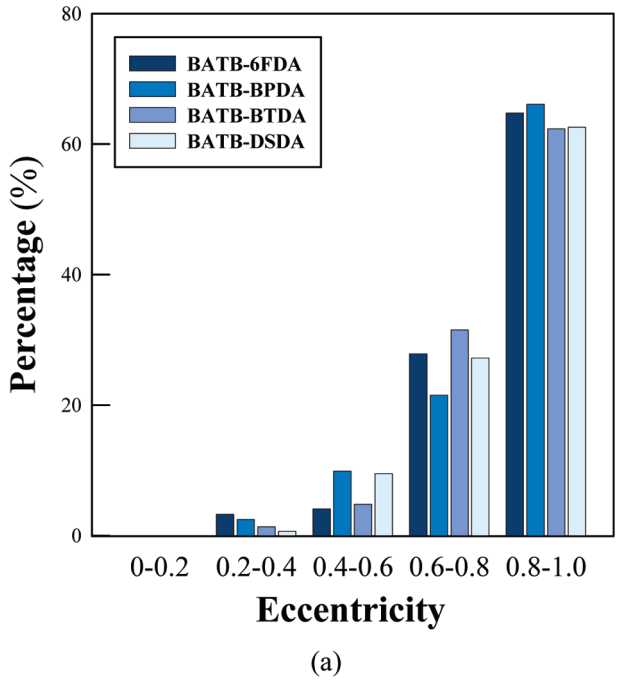

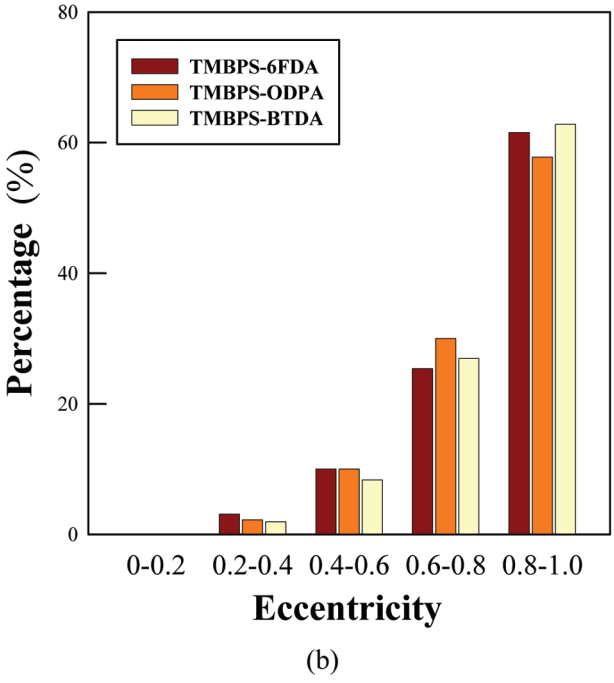

Figure 7. The distribution of free volume equivalent eccentricity of (a) BATB-based PI membranes and (b) TMBPS-based PI membranes.

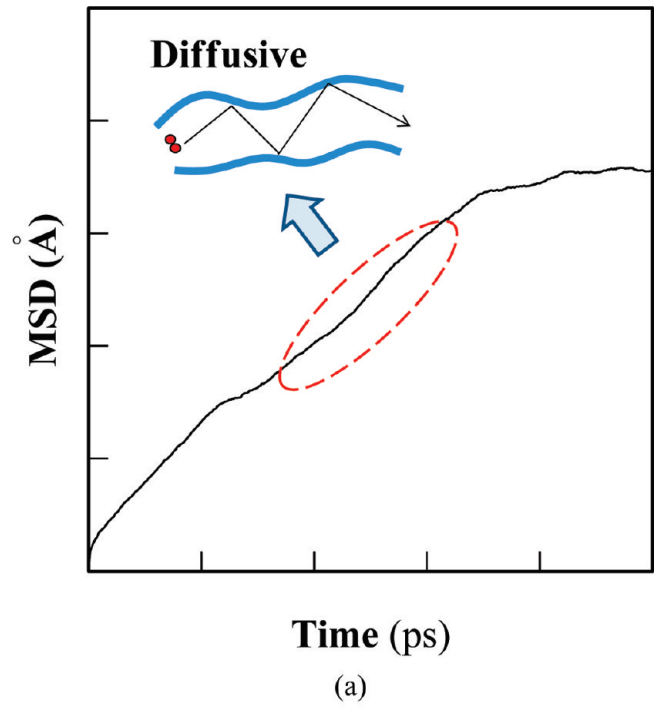

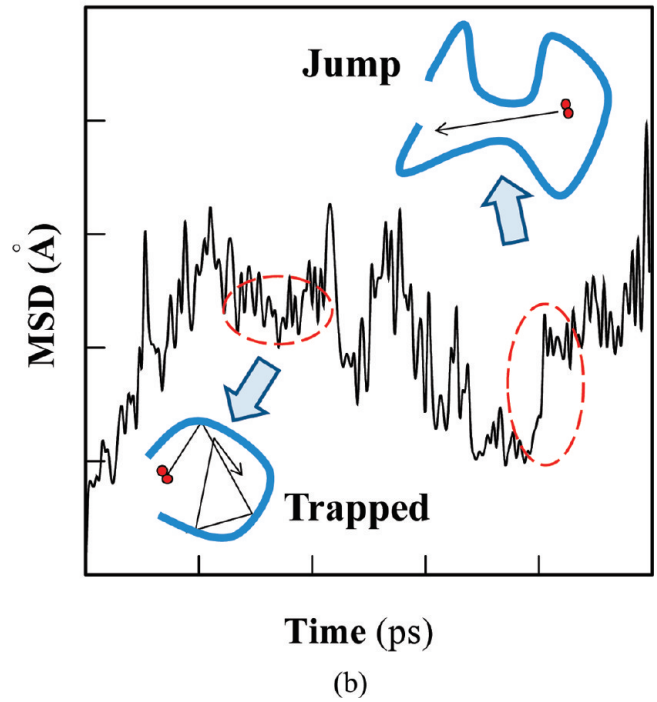

Figure 8. The scheme of gas molecular thermal motions in a polymeric membrane; (a) diffusive motion and (b) jumping and trapped motions.

of 3−6 Å than did the TMBPS−ODPA. These higher D_{eq} values of free volume suggest that the TMBPS−BTDA contained much larger or more continuous free volume elements in the membrane, resulting in larger FAV values. Furthermore, by comparing the BATB−6FDA and TMBPS−6FDA via FVSD analysis, we found that the TMBPS−6FDA had a much higher percentage of free volume D_{eq} values above 3 Å. The same tendency was seen for BATB−BTDA and TMBPS−BTDA. The greater number of free volume elements with larger D_{eq} values in the TMBPS-based PI membranes shows that the bulky TMBPS group exerted more influence on the development of high-flux gas separation membranes. For a qualitative analysis, Figure 6 shows the cross-sectional images of the BATB-based and TMBPS-based PI membrane models. A tendency in the free volume size similar to that mentioned above was also observed.

In addition to the free volume size distribution, the shape of the free volume elements could also affect the gas transport. Figure 7 shows the distribution of free volume E_{eq} values of the BATB-based and TMBPS-based PI membranes. As seen in Figure 7a, the BATB−6FDA PI membrane had more E_{eq} values in the range of 0.2−0.4. This tendency indicates that the free volume element of the BATA−6FDA PI membrane tended to approach a more circular shape in the membrane matrix, as compared to all of the other membranes. It was suggested that

TABLE 3: Time-Averaged Probability of O_2 Molecule Thermal Motions in the PI Membranes

	BATB−6FDA	BATB− BPDA	BATB− BTDA	BPDA−DSDA	TMBPS−6DFA	TMBPS−ODPA	TMBPS−BTDA
$P_{diffusive}$ (%)	1.00	0.00	0.00	0.00	1.00	0.00	0.00
$P_{jumping}$ (%)	88.00	90.00	97.00	97.00	91.00	95.00	95.00
$P_{trapped}$ (%)	11.00	10.00	3.00	3.00	8.00	5.00	5.00

the PI membranes containing 6FDA groups provided a larger free volume with a higher probability of forming a circular shape, which assisted in gas molecule penetration. In the case of E_{eq} values nearing unity, the free volume tended to be too narrow to form effective free space, even with a larger D_{eq} value. Thus, the free volume shape might be one of the factors controlling gas permeation. We also observed the same tendency in the case of the TMBPS-based PI membranes, as shown in Figure 7b.

3.3. Gas Diffusion Mechanism. From the solution-diffusion model, the gas transport mechanisms in the polymeric membranes were classified as sorption and diffusion behaviors. The gas diffusion mechanism in the PI membranes was investigated and then compared with the free volume distribution. Later, the gas sorption was also investigated to understand the effect of bulky groups on gas permeation.

The diffusion behaviors of gas molecules in polymeric membranes were mainly controlled by their thermal motions. These thermal motions were categorized into three types, diffusive, jumping, and trapped motion. The diffusive and jumping motions were considered as effective thermal motions for the diffusion mechanisms, as shown in Figure 8. Thus, we analyzed the time-averaged probability of O_2 molecule thermal motions in the PI membrane diffusion mechanism analysis, as shown in Table 3. It was observed that the O_2 molecules in the PI membranes had almost more than 90% ineffective thermal motion (trapped). In this situation, the appearance of diffusive motion or jumping would become relatively important for gas diffusion. As seen in Table 3, it was found that the PI membranes containing the 6FDA group had obviously more diffusive and jumping motions. It was inferred that the larger or more continuous free volume contributed to the effective thermal motion, enhancing gas diffusion. We also found similar tendencies for O_2 and N_2 permeability and diffusivity in the experimental data from Wang et al.[17]

3.4. Gas Sorption Behavior. The gas sorption isotherms of O_2 and N_2 were calculated to analyze the effect of a bulky group on gas sorption behaviors, as shown in Figures 9 and 10. By observing the sorption isotherms, it was found that the O_2 and N_2 sorption followed the behavior of Henry's law at lower pressures. The gas molecules were absorbed in the equilibrium free volume of the membranes. This sorption can be related to the operation pressures by a linear expression, as follows

$$C_D = K_D p \tag{9}$$

where C_D is Henry's law solubility of the absorbed gas, K_D is Henry's law solubility constant, and p is the surrounding pressure. In addition, the sorption mode of O_2 and N_2 was changed to the Langmuir mode by elevating the operating pressures. In the Langmuir sorption mode, the gas was assumed to be sorbed into the free space of the intrapolymer chains (excess free volume elements). These free volume elements are limited and are relatively small, as compared to the equilibrium free volume. Thus, the sorption behavior will cease once the sorption sites are saturated. The Langmuir-type isotherm can be approximated by the following equation

$$c_H = \frac{c_H' bp}{1 + bp} \tag{10}$$

where C_H is the Langmuir mode concentration of the absorbed gas, C_H' is the saturated concentration at which all excess

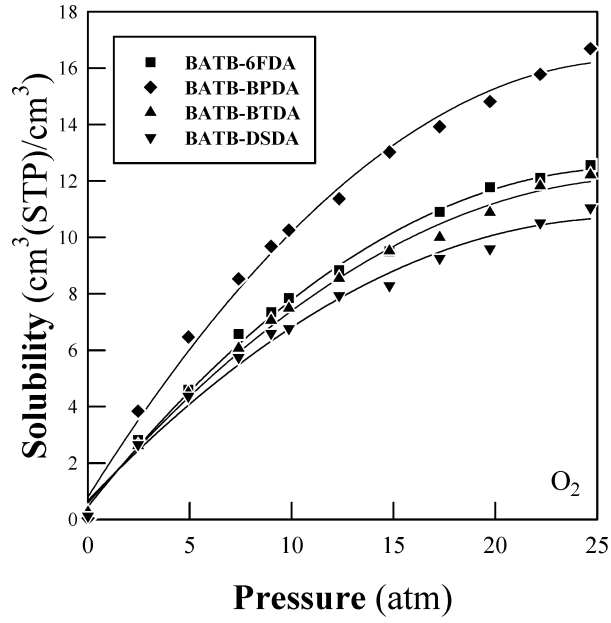

Figure 9. The O_2 and N_2 sorption isotherms of BATB-based PI membranes at different pressures at 308 K.

free volume sites are filled, b is the Langmuir affinity constant, and p is the operation pressure. These various sorption modes indicate that the sorption behaviors of O_2 and N_2 in our membrane models belong to the dual-sorption model, which agrees with the gas sorption behavior in glassy polymeric membranes. This behavior of the dual-sorption model observed in our simulated work is also found in the report of Wang et al.[17]

As shown in Figure 9, we found that the tendency of O_2 sorption in various PI membranes coincided with the FAV and FVSD analyses. The PI membrane containing the 6FDA group clearly had a higher solubility coefficient than all of the other membranes. This similarity between sorption and free volume analyses suggests that the larger and more continuous free space in the membranes provided more sites for gas sorption, resulting in higher solubility coefficients. In addition, we observed the same results in the case of the TMBPS-based PI membranes, as shown in Figure 10.

TABLE 4: Comparison of Simulated and Experimental Results of O_2 in BATB-Based and TMBPS-Based PI Membranes at 308 K and 9 atm

	solubility coefficient (cm^3(STP/cm^3atm))	
PI membrane	simulated value	experimental value[a]
BATB−6FDA	1.08	0.6
BATB−BPDA	0.82	0.4
BATB−BTDA	0.78	0.4
BATB−DSDA	0.73	0.3
TMBPS−6FDA	0.97	0.5
TMBPS−ODPA	0.73	0.5
TMBPS−BTDA	0.76	0.4

[a] From Wang et al.[17]

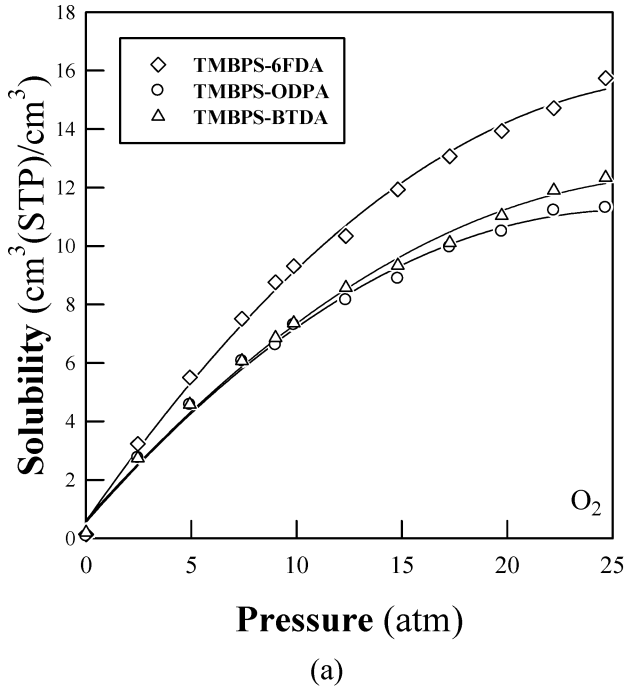

Figure 10. The O_2 and N_2 sorption isotherms of TMBPS-based PI membranes at different pressures at 308 K.

The solubility coefficients of O_2 and N_2 were also compared in this study in Figure 9. The O_2 solubility coefficients were 1.5−2 times larger than the N_2 solubility coefficients. This stresses that the sorption behaviors of various gas molecules in the PI membranes can be well simulated by the molecular models built in this work. Moreover, we also compared our simulated solubility coefficients with the experimental results from Wang et al.,[17] as listed in Table 4. Our simulated solubility coefficients were about 2 times larger than the experimental results. The reasons for the differences between the simulation and experimental work can be illustrated as follows: (a) the dimension of the simulated model and the MD duration adopted in this work were much less than that of the real system due to our present limited computational resources and (b) some intrinsic errors in the calculation process might still be produced by the selected force field optimized from the semiempirical equations.[33,34] In addition, on the basis of past literature, a variance between the simulated and experimental results of less than a factor of 3−5 seems to be acceptable.[14,23]

From the gas transport analyses, it was suggested that the bulky group in the membrane matrix enlarges the free volume elements and then promotes gas diffusion and sorption behaviors. The molecular simulation technique also proved to be a potential method for gaining insight into the use of membranes for gas separation at the microscale.

4. Conclusions

The membrane free volume and gas transport mechanisms of PI membranes composed of different diamines and dianhydrides were investigated using MD and MC techniques. The bulky 6FDA group in the PI membranes hindered the polymer chain packing, thus producing much more free volume inside. The FAV and free volume morphology analyses showed that the existence of the 6FDA group contributes to the formation of larger, continuous, and more circular effective free volume elements for gas passage. The diffusion mechanism analysis revealed that the PI membranes containing a 6FDA group provided more free space to promote more effective thermal motion, such as diffusive and jumping motions, contributing to the higher permeability. Furthermore, the greater effective free volume in the PI membranes composed of the 6FDA group also supplied more sites for gas sorption.

In summary, the bulky 6FDA group in the PI membranes enlarged the effective free volume, which promoted the effective thermal motion and sorption of gas molecules and affected the

gas permeability. The good agreement between simulated and experimental results suggests that the molecular simulations are potential techniques for improving our understanding of gas separation membranes.

Acknowledgment. The authors would like to express their appreciation to the National Science Council (NSC), the Center-of-Excellence (COE) Program on Membrane Technology from the Ministry of Education (MOE), R.O.C., and the project Toward Sustainable Green Technique at the Chung Yuan Christian University, Taiwan, under Grant CYCU-97-CR-CE, for their financial support. Computational calculation support from the National Center for High-Performance Computing, which provided the SGI O3800 computer and Cerius^2 software, is also greatly appreciated.

References and Notes

(1) Brown, P. J.; East, G. C.; McIntyre, J. E. *Polym. Commun.* **1990**, *31*, 156.
(2) Bi, J.; Simon, G. P.; Yamasaki, A.; Wang, C. L.; Kobayashi, Y.; Griesser, H. J. *Radiat. Phys. Chem.* **2000**, *58*, 563.
(3) Hu, C. C.; Ruaan, R. C.; Lai, J. Y. *J. Chin. Inst. Chem. Eng.* **2003**, *34*, 101.
(4) Bi, J. J.; Wang, C. L.; Kobayashi, Y.; Ogasawara, K.; Yamasaki, A. *J. Appl. Polym. Sci.* **2003**, *87*, 497.
(5) Kruczek, B. *J. Appl. Polym. Sci.* **2003**, *88*, 1100.
(6) Shao, L.; Chung, T. S.; Wensley, G.; Goh, S. H.; Pramoda, K. P. *J. Membr. Sci.* **2004**, *244*, 77.
(7) Fu, Y. J.; Hu, C. C.; Qui, H. z.; Lee, K. R.; Lai, J. Y. *Sep. Purif. Technol.* **2008**, *62*, 175.
(8) Joly, C.; Le Cerf, D.; Chappey, C.; Langevin, D.; Muller, G. *Sep. Purif. Technol.* **1999**, *16*, 47.
(9) Tung, K. L.; Lu, K. T. *J. Membr. Sci.* **2006**, *272*, 37.
(10) Tung, K. L.; Lu, K. T.; Ruaan, R. C.; Lai, J. Y. *Desalination* **2006**, *192*, 391.
(11) Tung, K. L.; Lu, K. T.; Ruaan, R. C.; Lai, J. Y. *Desalination* **2006**, *192*, 380.
(12) Chang, K. S.; Hsiung, C. C.; Lin, C. C.; Tung, K.-L., *J. Phys. Chem. B* **2009** *113*, doi: 10.1021/jp900246p.
(13) Min, K. E.; R., P D. *J. Polym. Sci., Pt. B: Polym. Phys.* **1988**, *26*, 1021.
(14) Hofmann, D.; Heuchel, M.; Yampolskii, Y.; Khotimskii, V.; Shantarovich, V. *Macromolecules* **2002**, *35*, 2129.
(15) Hirayama, Y.; Yoshinaga, T.; Kusuki, Y.; Ninomiya, K.; Sakakibara, T.; Tamari, T. *J. Membr. Sci.* **1996**, *111*, 169.
(16) Hirayama, Y.; Yoshinaga, T.; Kusuki, Y.; Ninomiya, K.; Sakakibara, T.; Tamari, T. *J. Membr. Sci.* **1996**, *111*, 183.
(17) Wang, Y. C.; Huang, S. H.; Hu, C. C.; Li, C. L.; Lee, K. R.; Liaw, D. J.; Lai, J. Y. *J. Membr. Sci.* **2005**, *248*, 15.
(18) Liu, S. L.; Wang, R.; Liu, Y.; Chng, M. L.; Chung, T. S. *Polymer* **2001**, *42*, 8847.
(19) Savoca, A. C.; Surnamer, A. D.; Tien, C. F. *Macromolecules* **1993**, *26*, 6211.
(20) Wright, C. T.; Paul, D. R. *Polymer* **1997**, *38*, 1871.
(21) Yampolskii, Y. P.; Korikov, A. P.; Shantarovich, V. P.; Nagai, K.; Freeman, B. D.; Masuda, T.; Teraguchi, M.; Kwak, G. *Macromolecules* **2001**, *34*, 1788.
(22) Yang, L.; Fang, J.; Meichin, N.; Tanaka, K.; Kita, H.; Okamoto, K. *Polymer* **2001**, *42*, 2021.
(23) Hofmann, D.; Maria, E.-C.; Lerbret, A.; Heuchel, M.; Yampolskii, Y. *Macromolecules* **2003**, *36*, 8528.
(24) Tiemblo, P.; Fernández-Arizpe, A.; Riande, E.; Guzmán, J. *Polymer* **2003**, *44*, 635.
(25) Tiemblo, P.; García, F.; García, J. M.; García, C.; Riande, E.; Guzmán, J. *Polymer* **2003**, *44*, 2661.
(26) Tiemblo, P.; Guzmán, J.; Riande, E.; García, F.; García, J. M. *Polymer* **2003**, *44*, 6773.
(27) Suzuki, T.; Yamada, Y.; Tsujita, Y. *Polymer* **2004**, *45*, 7167.
(28) Wang, L.; Cao, Y.; Zhou, M.; Liu, Q.; Ding, X.; Yuan, Q. *Eur. Polym. J.* **2008**, *44*, 225.
(29) Smit, E.; Mulder, M. H. V.; Smolders, C. A.; Karrenbeld, H.; van Eerden, J.; Feil, D. *J. Membr. Sci.* **1992**, *73*, 247.
(30) Gee, R. H.; Boyd, R. H. *Polymer* **1995**, *36*, 1435.
(31) Hofmann, D.; Fritz, L.; Ulbrich, J.; Schepers, C.; Bning, M. *Macromol. Theory Simul.* **2000**, *9*, 293.
(32) Heuchel, M.; Hofmann, D. *Desalination* **2002**, *144*, 67.
(33) Soldera, A. *Polymer* **2002**, *43*, 4269.
(34) Lim, S. Y.; Tsotsis, T. T.; Sahimi, M. *J. Chem. Phys.* **2003**, *119*, 496.

JP903551H